Article

Urban Heat on Hold: A Remote Sensing-Based Assessment of COVID-19 Lockdown Effects on Land Surface Temperature and SUHI in Nowshera, Pakistan

Waqar Akhtar [1,2,*], Jinming Sha [1,2,*], Xiaomei Li [3], Muhammad Jamal Nasir [4], Waqas Ahmed Mahar [5,6], Syed Hamid Akbar [7], Muhammad Ibrahim [8] and Sami Ur Rahman [1]

1   School of Geographical Sciences & School of Carbon Neutrality Future Technology, Fujian Normal University, Fuzhou 350117, China; samiurrahman418@gmail.com
2   Research Center of Sino-Europe Environmental Management and Landscape, Fujian Normal University, Fuzhou 350117, China
3   College of Environmental and Resource Sciences & College of Carbon Neutral Modern Industry, Fujian Normal University, Fuzhou 350117, China; lixiaomei@fjnu.edu.cn
4   Department of Geography & Geomatics, University of Peshawar, Peshawar 25000, Pakistan; drjamal@uop.edu.pk
5   Department of Architecture, School of Art, Design and Architecture (SADA), National University of Sciences and Technology (NUST), Islamabad 44000, Pakistan; waqas.mahar@sada.nust.edu.pk
6   Sustainable Building Design (SBD) Lab, Department of Urban & Environmental Engineering (UEE), Faculty of Applied Sciences, Université de Liège, 4000 Liège, Belgium
7   Faculty of Architecture & Arts, Hasselt University, 3500 Hasselt, Belgium; syedhamid.akbar@uhasselt.be
8   Department of Urban and Regional Planning, University of Peshawar, Peshawar 25000, Pakistan; plnr.ibrahim1@gmail.com
*   Correspondence: waqar.pukhtoonyar@gmail.com (W.A.); jmsha@fjnu.edu.cn (J.S.)

Abstract

The COVID-19 pandemic presented an unprecedented opportunity to assess the environmental effects of reduced anthropogenic activity on urban climates. This study investigates the impact of COVID-19-induced lockdowns on land surface temperature (LST) and the intensity of the surface urban heat island (SUHI) in Nowshera District, Khyber Pakhtunkhwa Province, Pakistan, which is experiencing rapid urbanization. Using Landsat 8/9 imagery, we assessed thermal changes across three periods: pre-lockdown (April 2019), during lockdown (April 2020), and post-lockdown (April 2021). Remote sensing indices, including NDVI and NDBI, were applied to evaluate the relationship between land cover and LST. Our results show a significant reduction in average LST during lockdown, from 31.38 °C in 2019 to 25.34 °C in 2020, a 6 °C decrease. Urban–rural LST differences narrowed from 9 °C to 6 °C. A one-way ANOVA confirmed significant differences in LST across the three periods ($F_{(2, 3)} = 3691.46$, $p < 0.001$), with Tukey HSD tests indicating that the lockdown period differed significantly from both the pre- and post-lockdown periods ($p < 0.001$). SUHI intensity fell from 35.10 °C to 28.89 °C during lockdown, then rebounded to 35.37 °C post-lockdown. The indices analysis shows that built-up and rangeland areas consistently recorded the highest LST (e.g., 35.36 °C and 37.09 °C in 2021, respectively), while vegetation and water bodies maintained lower temperatures (34.68 °C and 32.69 °C in 2021). NDVI confirmed the cooling effect of green areas, while high NDBI values correlated with increased LST in urban areas. These findings underscore the impact of human activity on urban heat dynamics and highlight the role of sustainable urban planning and green infrastructure in enhancing climate resilience. By exploring the relationships among land cover, anthropogenic activity, and urban climate resilience, this research offers policymakers and urban planners' valuable insights for developing adaptive, low-emission cities amid rapid urbanization and climate change.

1. Introduction

Urbanization is one of the significant processes of transforming the Earth's surface, changing land use and land cover in ways that disturb the urban thermal environment [1,2]. The well-documented phenomenon arising from urbanization is the higher temperature of urban areas than their rural surroundings, known as UHI (Urban Heat Island) [3]. This temperature variation is driven by various factors, including the replacement of natural vegetation with hard surfaces, reduced evapotranspiration, and increased emissions from vehicles, industries, and buildings due to anthropogenic activities [4]. The UHI exacerbates environmental and social challenges, including increased energy consumption, heightened vulnerability to heat waves, and degraded air quality [5]. The effect of UHI has gained global attention due to its direct implications for public health and urban sustainability [6]. The rapid urbanization in developing countries has intensified the effects of UHI in urban areas, where infrastructure development often outpaces the measures of climate adaptation [7]. Similarly, only 2% of the Earth's surface is occupied by cities, yet they account for 70% of global energy consumption and 75% of greenhouse gas emissions [8]. Therefore, understanding and mitigating the effects of UHI has become a cornerstone for sustainable development strategies.

Globally, China, India, and European countries have observed a drop in the concentration of NO_2 up to 30%, which has helped to reduce the impact of the UHI by minimizing the land surface temperature [9]. It shows the impact on the region's climate by decreasing human activity. For example, there has been a noticeable drop in LST due to reduced emissions [10]. This noticeable drop in LST has provided a natural experiment to examine the dynamics of urban thermal behavior during reduced human activity. It has yielded insights into sustainable urban design and climate adaptation techniques.

The Coronavirus Disease 2019 (COVID-19) began in late 2019. It provided a unique opportunity to examine the urban heat island and its relationship with human activities and land surface temperature (LST). Lockdowns implemented across the world to stop the virus's spread significantly decreased industrial activity, transportation, and other human-caused activities, which had a significant impact on the environment [11]. These measures drastically reduced the use of fossil fuels and enhanced air quality [12]. A cleaner, calmer urban environment resulted from the suspension of commercial activity, which also reduced noise pollution and vehicle emissions [9]. Specifically, the transportation systems experienced unprecedented disruptions, leading to reduced traffic flow and mobility, as also highlighted in recent studies on urban traffic prediction and management during pandemics [13].

The dynamics of urban heat, particularly land surface temperature (LST) and surface urban heat island (SUHI) intensity, have been widely studied in large metropolitan regions worldwide. Several studies from megacities of high-population countries, such as Karachi, Lahore, Delhi, Beijing, and New York, highlight how urbanization and anthropogenic activity exaggerate the thermal environments of these cities [14,15]. However, the rapidly urbanizing secondary cities remain underrepresented in this discourse, despite experiencing rapid population growth and unregulated urban expansion that make them equally vulnerable to heat-related hazards. The COVID-19 lockdown period from 2019 to 2021 created an unprecedented opportunity to observe how sudden reductions in anthropogenic activity—such as transport, industry, and commercial operations—affect urban thermal

behavior [16]. While recent studies from global metropolises such as Wuhan, Delhi, and Karachi have documented cooling effects during lockdown periods, evidence from secondary cities in Pakistan remains undocumented. This gap is critical, as smaller urban centers host significant populations, yet lack the adaptive infrastructure and planning frameworks available in larger cities.

Cities can moderate their thermal environment through planning and management measures; failing to account for these interventions obscures the extent to which LST changes observed are driven by land-cover conversion rather than policy or design choices. Recent studies show that urban management strategies, especially the provision and design of green infrastructure, land-use zoning, and modifications to urban morphology, produce measurable cooling effects at neighbourhood-to-city scales. Small-to-medium green patches and connected green corridors can lower air and surface temperatures by about 1–3 °C locally, and larger, well-distributed green networks deliver larger cooling and public-health benefits [17,18]. Similarly, managing impervious-surface extent and spatial configuration through compact mixed land use, protected green patches, and lower-albedo materials reduces daytime LST, while three-dimensional urban form (building density, height, and sky-view factor) controls radiative exchanges that amplify or mitigate surface heating [19]. Finally, multiple recent spatiotemporal analyses demonstrate that trajectories of LULC change, the timing, rate, and spatial pattern of built-up expansion, vegetation loss, and water-body change, strongly determine LST trends and SUHI development in mid-sized and secondary cities [3]. Together, these findings imply that assessing lockdown-related LST changes without considering concurrent land-use dynamics and management strategies gives an incomplete picture; integrating policy-relevant explanations strengthens both the interpretation and the planning relevance of LST results [20,21].

This study addresses that gap by focusing on Nowshera City, a mid-sized urban centre in Khyber Pakhtunkhwa, Pakistan, which has not been previously studied in terms of SUHI dynamics. This is the first empirical investigation to evaluate how movement restrictions during the COVID-19 lockdown influenced LST and SUHI in a secondary city in Pakistan. By linking mobility restrictions with local-scale heat dynamics, the study provides novel insights into how reductions in anthropogenic activity translate into measurable cooling effects.

Beyond academic contribution, the findings carry important policy implications. For example, if temporary reductions in human activity can yield noticeable thermal improvements, sustainable planning measures—such as green infrastructure provision, regulated transport emissions, and controlled urban expansion—could play a decisive role in mitigating SUHI effects. Thus, this study not only fills a geographical and thematic research gap but also provides evidence-based lessons for heat-resilient urban planning in developing countries.

The Nowshera district, with a semi-arid climate and rapidly urbanizing terrain, is of concern because it is undergoing significant changes in land use and land cover (LULC) driven by fluctuations in urbanization and population. The semi-arid climatic setting of the district, with its unique combination of urban, agricultural, and riverine areas, makes it an ideal location to explore the nexus between human heat emissions and LULC changes within urban thermal dynamics.

This paper explores how the COVID-19 lockdown affected LST and SUHI intensity in Nowshera, providing insight into the effects of reduced human activities on an urban environment. By considering such variations, the study contributes to broader research on the relationship between human activity and the dynamics of urban thermal fields. The results are thus highly relevant to designing areas that are resilient and sustainable and able to cope with the double onslaught of rapid urbanization and climate change.

2. Study Area and Methods

2.1. Geographic Context

Nowshera district lies in the province of Khyber Pakhtunkhwa, Pakistan, and has a semi-arid climatic condition. Its total area is approximately 1748 km². The dominant land uses/land cover are built-up areas, agriculture, and water bodies. District Attock lies to the east, and Districts Peshawar and Charsadda lie to the west and northwest of Nowshera. The northern side contains the districts of Mardan and Swabi, and to the southern side lies the Kohat district. The Nowshera district is located between longitudes 72°16′15″ E and latitudes 33°41′30″ to 34°10′15″ N. As per the 2017 Census, it has a population of approximately 1.5 million. Nowshera district has two major rivers: The River Kabul and the River Indus. The Kabul River enters the district from the west through Kund Khairabad and merges with the River Indus. The drainage network of the district is characterized by several annual dry torrents joining the Kabul River from the south [22]. Figure 1 illustrates the location of the study area.
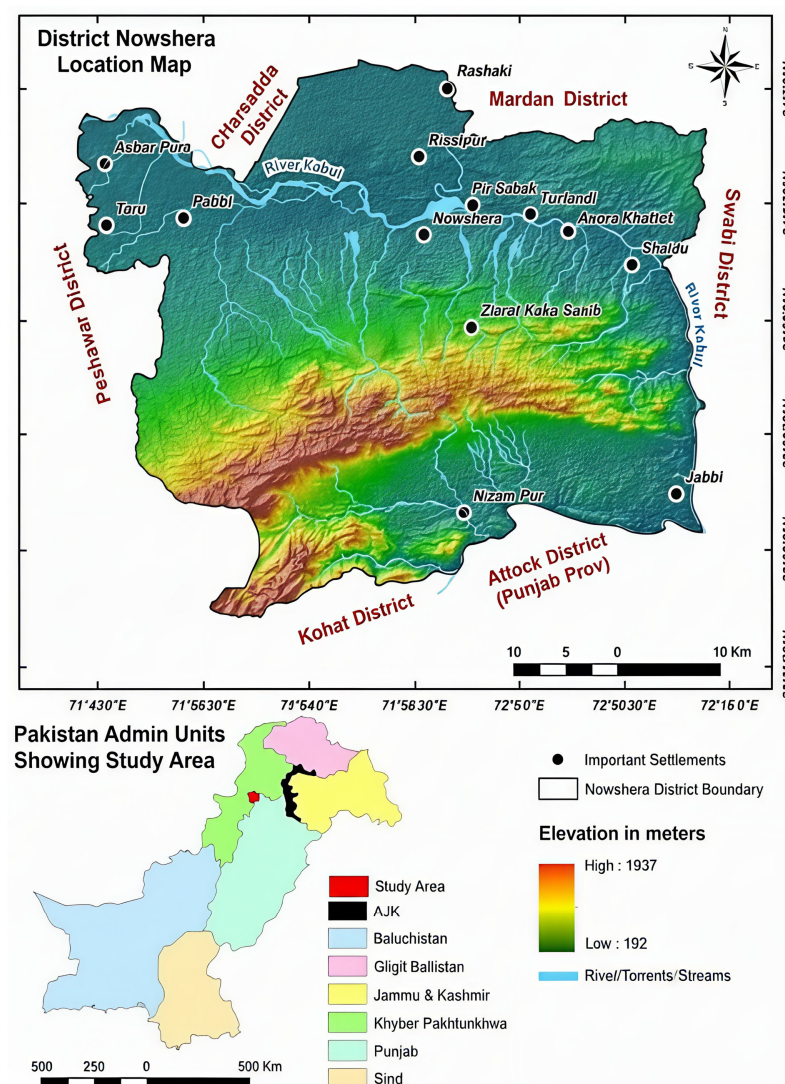

Figure 1. Location Map of the Study Area.

2.2. Climatic Characteristics

Nowshera has a semi-arid climate with apparent seasonal variations that profoundly affect its environment and land-use patterns. Summers are hot, typically from May to September, when temperatures often reach 40 °C or higher. The hottest month is usually

June, with an average maximum temperature of 33.6 °C. These conditions and low relative humidity make it a challenging environment for human activity and vegetation, especially in urban areas, where the surface urban heat island (SUHI) effect intensifies heat. Winters fall between November and February, with January the coldest month, with an average minimum of 10.1 °C. These months are relatively cooler, offering temporary respite from summer's intensity, sometimes boosted by moderate rainfall that benefits agriculture. Rainfall in Nowshera is somewhat irregular, and the bulk of the annual precipitation falls during the monsoon season of July–September, peaking in August with 112 mm. The driest month is October with only 13 mm. The diurnal range is also noteworthy, with significant increases during months of transition, such as March and October, due to clear skies and low atmospheric moisture. These climatic features shape Nowshera's land use, vegetation, and urban thermal behavior, which, in turn, influence the city's climatic vulnerability and resilience capacity.

2.3. Data Collection

Based on the study objective, data were collected from multiple sources, including primary and secondary sources and remote sensing technology. The data sources and their specific applications are described below:

a.   Satellite Data:

The thermal bands of Landsat 8 (Bands 10) were acquired from the USGS Earth Explorer platform (https://earthexplorer.usgs.gov/, accessed on 22 November 2025) [23]. This data was used to determine the Land Use/Land Cover (LULC), land surface temperature (LST), and Normalized Difference Vegetation Index (NDVI), Normalized Difference Built-up Index (NDBI), and Normalized Difference Water Index (NDWI). Data were selected between the years 2019 through 2020, and 2021 to capture all three periods: pre-lockdown, lockdown, and post-lockdown. Table 1 depicts the satellite imagery acquisitions of this study.

Table 1. Landsat 8 Acquisition Details for Nowshera (2019–2021).

Year	Acquisition Date	Sensor	Path/Row	Spatial Resolution	Description
2019	18 April 2019	Landsat 8 OLI/TIRS	152/38	30 m (TIR 100 m resampled)	Pre-lockdown period
2020	14 April 2020	Landsat 8 OLI/TIRS	152/38	30 m	Lockdown period
2021	08 April 2021	Landsat 8 OLI/TIRS	152/38	30 m	Post-lockdown period

Source: USGS Earth Explorer, https://earthexplorer.usgs.gov/, accessed on 22 November 2025 [23].

MODIS thermal band data, available through Google Earth Engine, were used further to validate the mean temperature for the three periods.

b.   Meteorological Data:

Mean maximum and minimum temperature data were also collected from the regional metrology office in Peshawar, the provincial capital of Khyber Pakhtunkhwa. The information on the lockdown was cross-checked against mean temperature measurements from 1–20 April 2020, in Nowshera.

c.   Lockdown Timeline:

In Pakistan, the first lockdown lasted from March 2020 to May 2020, during which significant reductions in human activity were observed.

2.4. Data Analysis

2.4.1. Land Use/Land Cover Change Detection

Land Use/Land Cover Change (LULCC) analysis was performed using supervised classification in ArcGIS 10.5. Five major land-cover classes were identified: built-up areas, vegetation, rangeland, water bodies, and agricultural land. Training samples for each class were manually digitized using high-resolution Google Earth imagery to ensure clear spectral representation. The Maximum Likelihood Classification (MLC) algorithm was applied to classify Landsat scenes for 2019, 2020, and 2021. After classification, land-cover maps for the three years were compared to identify changes in urban expansion, vegetation loss, and shifts in other land-cover types. This multi-year comparison allowed a clear assessment of LULC dynamics over the pre-lockdown, lockdown, and post-lockdown periods.

Land Cover Classification Accuracy Assessment

Classification accuracy was evaluated using an independent validation set. A confusion matrix was produced to compute overall accuracy and the Kappa coefficient. The overall classification accuracies were 89.4% in 2019, 91.2% in 2020, and 90.6% in 2021, with corresponding Kappa coefficients of 0.87, 0.89, and 0.88, respectively. These values indicate strong agreement between the classified outputs and reference data and meet the generally accepted accuracy thresholds for LULC studies.

2.4.2. Land Surface Temperature (LST) Estimation

Land surface temperature (LST) estimation models are vital for assessing the thermal characteristics of Earth's surface, particularly for environmental monitoring and urban planning. These models typically utilize remote sensing data, particularly from satellites like Landsat, to derive surface thermal characteristics and temperatures through thermal infrared bands [24]. The estimation process often involves converting digital numbers from satellite imagery into radiance and then into brightness temperature, followed by applying algorithms that account for atmospheric effects [25]. Accurate LST estimation is crucial for understanding land cover changes, urban heat island effects, and climate variations, enabling informed decision-making for sustainable land management and urban development [26].

The Landsat 8 thermal and optical bands for 2019, 2020, and 2021 were processed in ArcGIS 10.5. The raw Level 1 images downloaded from USGS EarthExplorer were converted to top-of-atmosphere (TOA) reflectance and spectral radiance using the calibration coefficients from the metadata file. Brightness temperature was computed from the thermal band (TIRS 10), followed by land surface emissivity estimation using NDVI. The final LST was extracted using the standard single-channel algorithm. Three Landsat scenes were used, corresponding to the pre-lockdown (18 April 2019), lockdown (14 April 2020), and post-lockdown (8 April 2021) periods.

LST was derived from Landsat thermal infrared data following standard algorithms:

i. Digital Numbers (DN) Conversion: Thermal bands (Band 10 and 11 for Landsat 8/9) were processed to convert DN values into spectral radiance using Equation (1).

$$TOA\ (L) = ML \times Qcal + AL \qquad (1)$$

where:

$ML = Band\ specific\ multiplicative\ rescaling\ factor\ from\ the\ meta\ data$
$(RADIANCE\_MULT\_BAND\_x,\ where\ x\ is\ the\ band\ number)$.

$Qcal = corresponds\ to\ band\ 10$
$AL = Band-specific\ additive\ rescaling\ factor\ from\ the\ metadata$
$(RADIANCE\_ADD\_BAND\_x, where\ x\ is\ the\ band\ number).$
$TOA = 0.0003342 * "Band\ 10" + 0.1$

ii. Brightness Temperature: Top-of-atmosphere (TOA) spectral radiance values were transformed into brightness temperature using Equation (2).

$$BT = (K2/\ (ln\ (K1/\ L) + 1)) - 273.15 \tag{2}$$

where:

$K1 =\ Band-specific\ thermal\ conversion\ constant\ from\ the\ metadata$
$(K1\_CONSTANT\_BAND\_x,\ where\ x\ is\ the\ thermal\ band\ number).$
$K2 =\ Band-specific\ thermal\ conversion\ constant\ from\ the\ metadata$
$(K2\_CONSTANT\_BAND\_x,\ where\ x\ is\ the\ thermal\ band\ number).$
$L =\ TOA$

To get the results in Celsius, the radiant temperature is therefore modified by adding absolute zero (roughly $-273.15\ °C$) from Equation (3).

$$BT = (1321.0789/Ln((774.8853/"\%TOA\%") + 1)) - 273.15 \tag{3}$$

iii. Normalized Difference Vegetation Index (NDVI): NDVI is frequently used to determine changes in the vegetation and to identify the cover of the vegetation [27]. Equation (4) is used to obtain it from the red and near-infrared (NIR) bands' reflectance [28].

$$NDVI = float\frac{(Band\ 5 - Band\ 4)}{(Band\ 5 + Band\ 4)} \tag{4}$$

The NDVI calculation is important because it requires estimating the vegetation proportion (Pv), which has a strong correlation with NDVI, and emissivity (ε), which is related to Pv.

iv. Proportion of Vegetation (Pv): Derived from NDVI values to estimate emissivity (Equations (5) and (7)).

$$Pv = Square\left(\frac{(NDVI - NDVImin)}{(NDVImax - NDVImin)}\right) \tag{5}$$

ArcGIS allows us to observe the NDVI minimum and maximum values within the image.

$$Pv = Square\left(\frac{("NDVI" - 0.216901)}{(0.632267 - 0.216901)}\right) \tag{6}$$

- Calculate Emissivity ε by employing Equation (7)

$$\varepsilon = 0.004 \times Pv + 0.986 \tag{7}$$

The 0.986 in the formula represents the equation's correction value.

- The land surface temperature was calculated by using Equation (8)

$$LST = \left(BT/\left(1 + \left(0.00115 \times \frac{BT}{1.4388}\right) \times Ln(\varepsilon)\right)\right) \tag{8}$$

where:

BT: Brightness Temperature, derived from satellite thermal bands, measured in Kelvin (K) ε: Land Surface Emissivity, derived from Equation (7).

To ensure seasonal consistency and minimize weather-related variability, a single cloud-free Landsat scene was selected for each year, all acquired within the same month (April). These images represent the closest available temporal match across the three periods. Although multi-date or seasonal composites can further reduce the influence of atmospheric conditions, suitable cloud-free images were limited in the study area. The selected scenes, therefore, provide the most consistent basis for comparison across the pre-, during-, and post-lockdown periods.

2.4.3. Indices

Different landscape types can be distinguished using various remote sensing indices [29]. In this study, NDBaI, NDBI, and NDWI indices were calculated to evaluate the influence of land-cover characteristics on LST. Zonal statistics were applied to extract mean LST values within NDVI, NDBI, and NDWI-defined zones. This allowed direct comparison between vegetation density, built-up intensity, moisture conditions, and surface temperature. Through this, we will underscore the impact of LST on the growth of the surface urban heat island. An evaluation of the correlation between LST, NDBI, NDVI, NDWI, and NDBaI will be conducted. These spectral indices are usually +1.0. The built-up areas, bare land, vegetation, and water surface are generally represented by the positive values of NDBaI, NDBI, NDVI, and NDWI, respectively [30].

i. Normalized Difference Built-up Index (NDBI): Measured to identify urban built-up areas using shortwave infrared and near-infrared bands (Equation (9)).

$$NDBI = float\ \frac{SWIR\ (b6) - NIR\ (b5)}{SWIR\ (b6) + NIR(b5)} \tag{9}$$

According to Zhao et al. (2003), the built-up area's spectral response shows more reflectance in the SWIR than in the NIR wavelength range [31].

ii. Normalized Difference Water Index (NDWI): Used to identify water bodies, employing visible green and shortwave infrared reflectance (Equation (10)). Equation (10) [32] indicates how to find the water using the Modified Normalized Difference Water Index. Availability in vegetation using the reflectance of visible green and Shortwave Infrared (Landsat-8):

$$MNDWI = float\frac{Green\ (b3) - SWIR(b6)}{Green\ (b3) - SWIR(b6)} \tag{10}$$

iii. Normalized Difference Bareness Index (NDBaI): Developed by Zhao and Chen (2005), this will be utilized to extract bare land from Landsat imagery [33]. Equation (11) will be used to derive it, utilizing Landsat-8's Thermal Infrared (band 10) and Shortwave Infrared (band 6) [34].

$$NDBai = float\ \frac{SWIR\ (b6) - TIR(b10)}{SWIR\ (b6) + TIR(b10)} \tag{11}$$

Correlations between LST and spectral indices (NDVI, NDBI, NDWI, and NDBaI) were assessed to evaluate the thermal impact of different LULC types. Positive values indicated built-up or bare land, while negative values represented vegetation or water bodies.

2.4.4. Statistical Analysis

The impact of the COVID-19 lockdown on land surface temperature (LST) was examined using a one-way Analysis of Variance (ANOVA). Three periods were compared: pre-lockdown (April 2019), during lockdown (April 2020), and post-lockdown (April 2021). To ensure consistent seasonal conditions, LST values were extracted from two dates in each year (April 1 and April 20), and the mean LST was calculated for each period.

Before applying ANOVA, the required assumptions were tested. Independence was ensured by selecting spatially non-overlapping sampling points. The normality of LST distributions was assessed using the Shapiro–Wilk test, while Levene's test was used to confirm homogeneity of variances. Both tests indicated that the assumptions were satisfied ($p > 0.05$), validating the use of ANOVA for group comparison.

The null hypothesis (H_0) stated that the mean LST does not differ across the three periods, while the alternative hypothesis (H_1) proposed that at least one period differs significantly. A *p*-value of <0.05 was used to evaluate statistical significance. When the ANOVA test indicated a significant difference, Tukey's Honestly Significant Difference (HSD) post hoc test was applied to identify which periods differed from one another.

All statistical analyses were conducted in IBM SPSS Statistics 30.0.0, which was used for assumption testing, ANOVA computation, and post hoc evaluation. This statistical approach provided a robust framework for detecting temporal LST differences and understanding the extent to which reduced human activity during the lockdown influenced surface temperatures.

This statistical method will provide a strong framework for understanding how the lockdown affects changes in land surface temperature. It will benefit us to identify temperature patterns across multiple periods, enabling a more thorough investigation of environmental dynamics and supporting broader debates on environmental and climatic changes driven by limited human activities. The results underline the need for statistical analysis in evaluating environmental changes and contribute to broader debates on climatic changes driven by human activity constraints. Furthermore, the research highlights the connection between lower anthropogenic activity and fluctuations in metropolitan heat, providing valuable insights for sustainable urban management and the development of future climate resilience.

2.4.5. Study of Surface Urban Heat Islands (SUHI)

Because this study derives heat island intensity directly from satellite-based LST, the analysis refers specifically to the surface urban heat island (SUHI), not to urban canopy or boundary-layer heat islands. Comparing regional temperature variations between urban and rural areas helped one to estimate the surface urban heat island (SUHI) effect. To compute the SUHI intensity, two key steps were followed:

1. Urban and Rural Reference Zone Selection:
   Urban areas were delineated using built-up land identified through supervised LULC classification. Rural reference zones were selected from non-urban areas dominated by vegetation and bare land, located outside the urban boundary but within the same climatic region to ensure comparability.
2. Zonal Statistics for LST Extraction:
   Average LST values for both urban and rural zones were extracted using zonal statistics. This enabled consistent comparison across homogeneous land cover categories.

The technique involved building land surface temperature (LST) distribution maps to identify urban thermal hotspots, therefore providing an unambiguous visual depiction of temperature variations over the study area. Zonal statistics helped to determine average LST values for specified urban and rural zones. At last, the temperature difference between

these zones was computed using Equation (12), therefore approximating the degree of SUHI. This multi-scale approach gave a more realistic evaluation of the SUHI effect and its geographical fluctuations.

$$\text{SUHI Intensity} = \text{LSTurban} - \text{LSTrural} \tag{12}$$

This approach provides a consistent and spatially explicit method for estimating SUHI magnitude and understanding its variation across the pre-lockdown, lockdown, and post-lockdown periods.

2.4.6. Uncertainty Considerations

Several sources of uncertainty are associated with satellite-derived LST, atmospheric correction, and LULC classification. For LST estimation, uncertainties may arise from sensor calibration, emissivity estimation, and atmospheric effects. To minimize these effects, the study used standard USGS-recommended radiometric and atmospheric correction procedures, along with land-cover-based emissive values. While residual atmospheric influence cannot be eliminated, using images from the same month (April) across all study years helps maintain temporal consistency.

In LULC classification, uncertainty may arise from spectral overlap among certain classes. The use of a supervised maximum likelihood classifier and validation through overall accuracy and the Kappa coefficient reduces classification error. The classification outputs in this study achieved acceptable accuracy levels for detecting major land-cover categories.

Although these uncertainties do not alter the main results, future studies may conduct sensitivity analyses or incorporate multi-source datasets to quantify them further and reduce their impact. Figure 2 illustrates the detailed methodology used in this study.
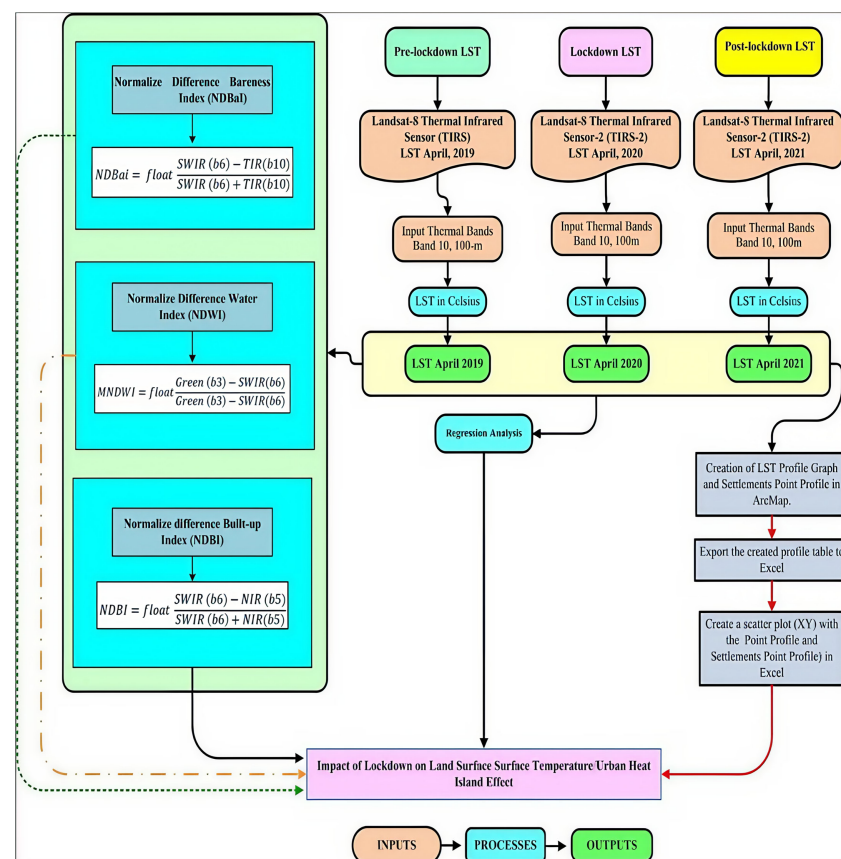

Figure 2. Research methodology flow chart for the study.

3. Results

This study determined land surface temperature (LST) differences and the formation of the surface urban heat island (SUHI) effect in the Nowshera district across three periods of the COVID-19 pandemic: before, during, and after the lockdown. Data analysis of pre- (2019), during (2020), and post- (2021) shows significant temperature variations within the urban agglomeration and between urban and rural areas, with the most significant cooling observed during the 2020 lockdown. The LST variations between urban centers, major roads, and rural areas highlight human activities, especially vehicular traffic, as significant drivers of changes in the thermal environment. The comparative analysis of LST before, during, and after the lockdown periods is shown in Figure 3, while Table 2 calculates the temperature differences. The analysis shows an intuitive relationship between reduced human activity during lockdown and the resulting reduction in urban temperatures. Figure 4 plots the pre-lockdown SUHI over the Nowshera district. The LST difference of 9 °C is experienced between urban downtown and suburban rural areas. A 6 °C difference between urban and rural areas was observed during the April 2020 lockdown. After the lockdown, a 7.5 °C difference in temperature was observed between urban and rural areas of Nowshera District.
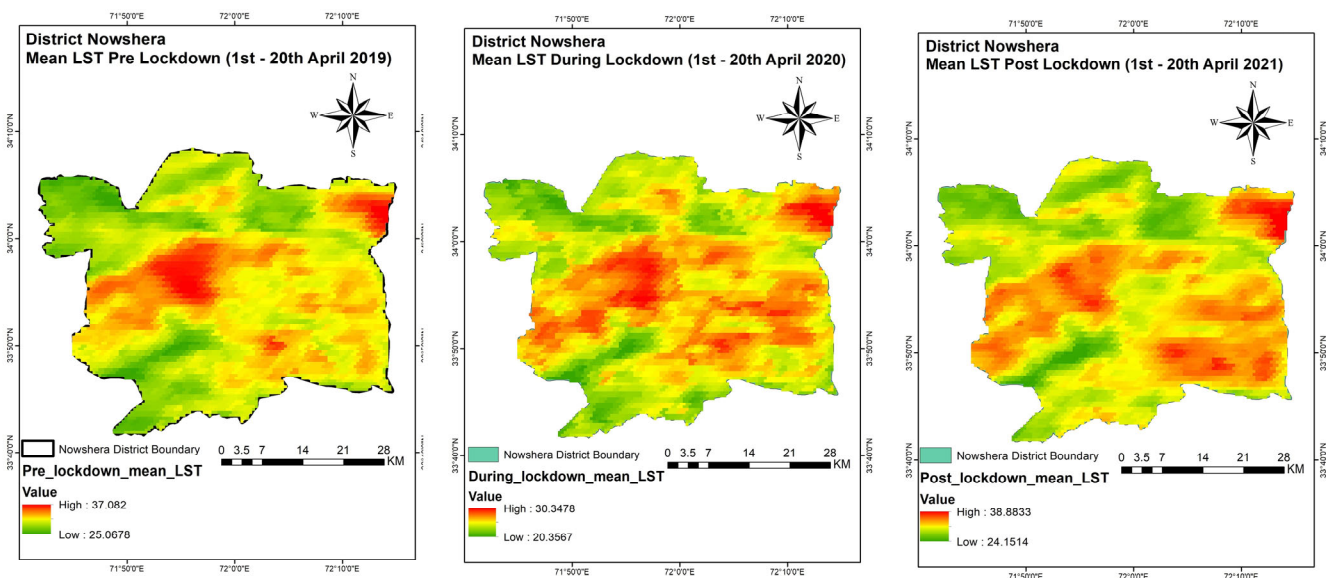

Figure 3. LST Trends Across Pre-, During-, and Post-Lockdown Phases in Nowshera District (April 2019–2021).

Table 2. LST for Nowshera District (1–20 April 2019, 2020 and 2021).

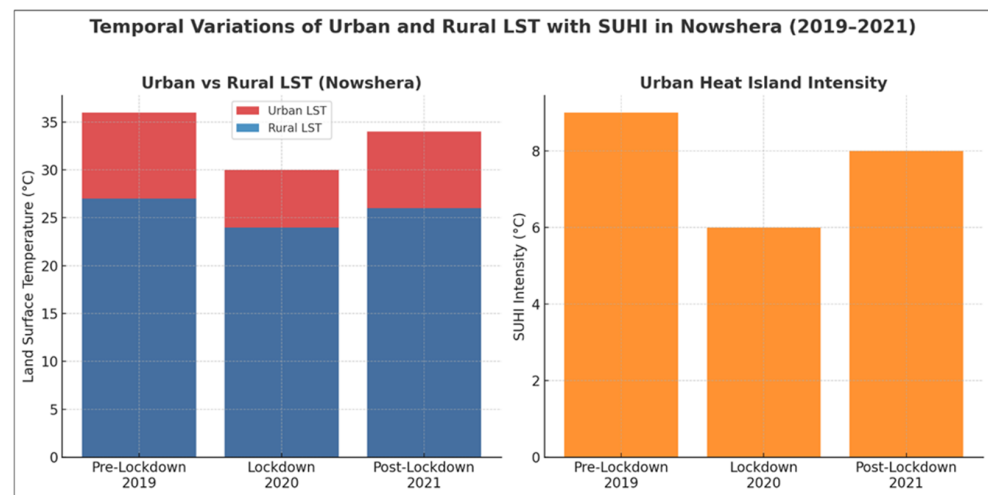| Date	Maximum LST	Minimum LST	Average LST (°C)	SD of LST (°C)
Pre-Lockdown April. 2019	37.08	25.68	31.38	5.65
During the lockdown in April. 2020	30.347	20.35	25.34	4.95
Post lockdown April. 2021	38.88	24.15	31.51	7.20

Figure 4. Surface Urban Heat Island (SUHI) Trends: Pre-Lockdown, Lockdown, and Post-Lockdown Periods (April 2019–April 2021).

3.1. The Land Surface Temperature of District Nowshera

The land surface temperature (LST) analysis was conducted from 2019 to 2021, using April of each year. This period was chosen to ensure continuity in seasonal and environmental conditions, therefore enabling a correct comparison of LST trends pre-lockdown, during lockdown, and post-lockdown. The findings show notable differences in the maximum and minimum mean LST during these eras, thereby highlighting the influence of human activities and environmental changes on surface temperatures. The average LST was 31.38 °C, with a standard deviation of 5.65 °C; the maximum LST was 37.08 °C, recorded before the COVID-19 lockdown in April 2019; the minimum LST was 25.68 °C. The high average LST and moderate SD reflect typical urban heat impacts resulting from pre-pandemic activity levels, including vehicle emissions, industrial operations, and reduced vegetation coverage.

The maximum and minimum LST values dropped during the COVID-19 lockdown in April 2020. With an average of 25.35 °C, the highest Mean LST dropped to 30.35 °C, a notable dip in LST, from the pre-lockdown period in 2019. Similarly, the minimum LST dropped from 5.33 °C to 20.35 °C. The decline in the standard deviation to 4.95 °C suggests more homogeneous temperatures across the region. The lower SD points to less anthropogenic heat generation, suggesting a reduced SUHI effect. The cessation of commercial operations, reduced vehicle traffic, and decreased anthropogenic heat emissions during the lockdown period helped explain this significant drop in LST. Moreover, better air quality and lower pollution levels most certainly contributed to explaining the cooling effect noticed during this period. Following the easing of lockdown restrictions in April 2021, LST values both maximum and minimum showed an increasing trend. While the minimum LST rose to 24.15 °C, somewhat below its pre-lockdown equivalent, the maximum LST rose to 38.88 °C, exceeding pre-lockdown values by 1.80 °C. Reflecting rising temperature variability, the average LST rebounded to 31.52 °C, and the standard deviation dropped considerably to 7.20 °C. The higher SD indicates more obvious temperature fluctuations. The rebound in LST values aligns with the resumption of regular economic and social activities, rising vehicle emissions, and ongoing urbanization trends. This post-lockdown increase emphasizes how much human activity shapes land surface temperatures. Table 2 and Figure 3 illustrate the thorough examination of the LST variances before, during, and after the COVID-19 lockdown.

3.2. Temporal Changes in SUHI

The SUHI analysis for Nowshera revealed clear temporal variations across the pre-lockdown (2019), lockdown (2020), and post-lockdown (2021) periods, as shown in Figures 4 and 5. During the pre-lockdown period (April 2019), the SUHI effect was strongly pronounced, with the inset profile graph showing an urban–rural temperature gradient of nearly 9 °C. The temperature dropped from approximately 36 °C in the urban core to 27 °C in the suburban northwest over a distance of 15 km, indicating significant heat accumulation in densely built-up zones with limited vegetation (Figure 5a).
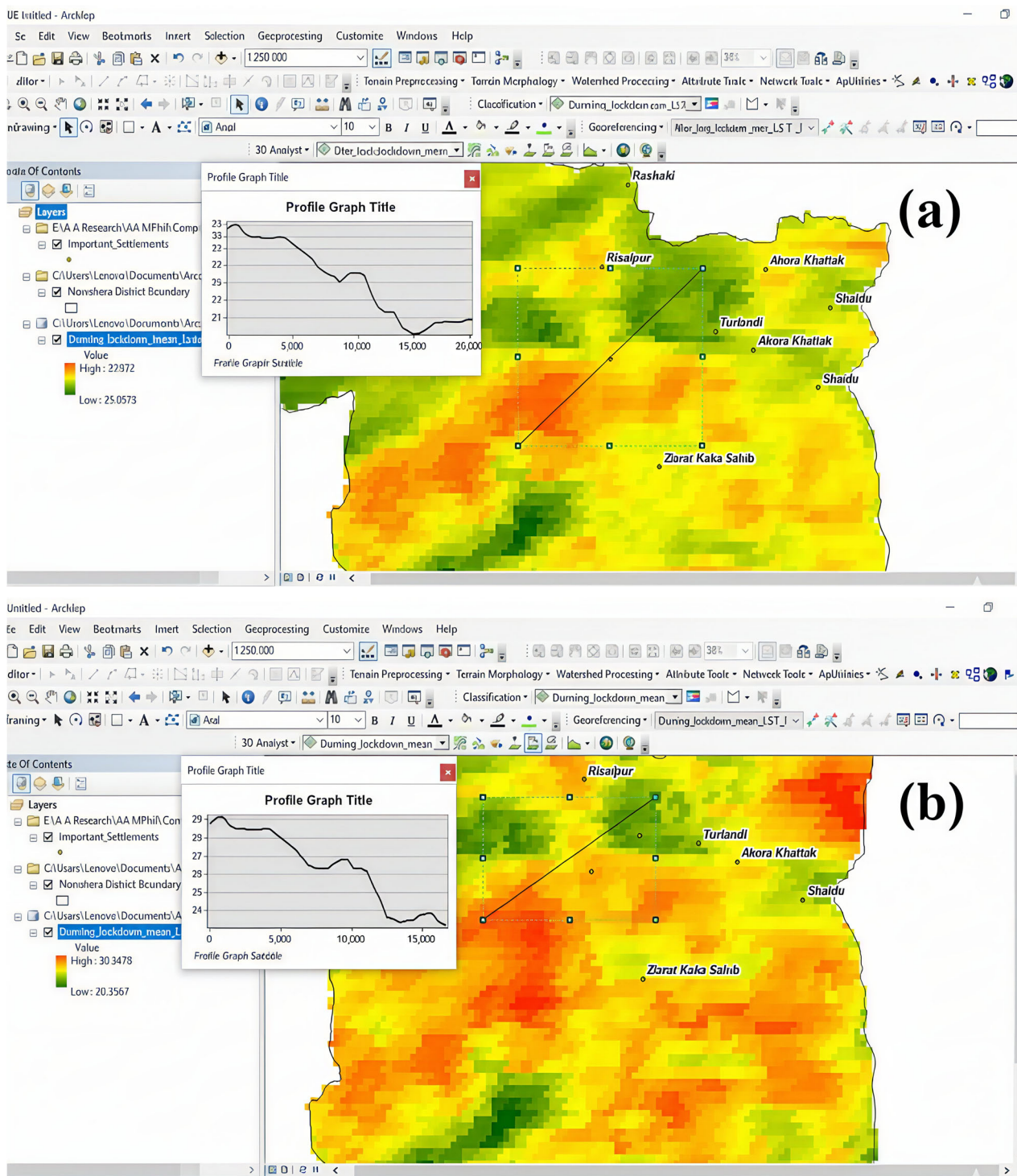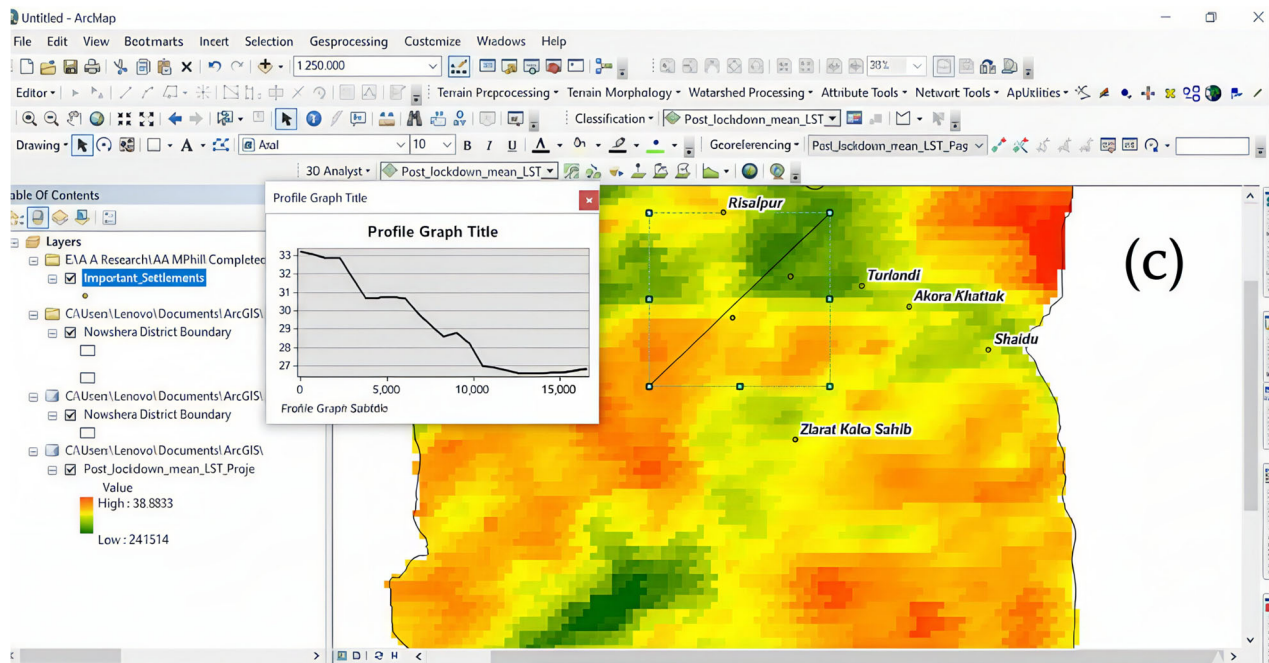

Figure 5. *Cont.*

Figure 5. It shows the spatial LST distribution, while the corresponding SUHI intensities were computed separately using the urban–rural LST (**a**) pre-lockdown 2019, (**b**) lockdown 2020, and (**c**) post-lockdown 2021.

In contrast, the lockdown period (April 2020) was characterized by a notable reduction in the SUHI effect. The temperature difference between urban and rural areas decreased to about 6 °C, with urban LSTs averaging 30 °C and rural zones registering around 24 °C. This decline reflects the cooling effect of reduced anthropogenic heat emissions due to restricted vehicular movement, industrial activities, and commercial operations (Figure 5b).

Following the easing of restrictions in the post-lockdown period (April 2021), the SUHI intensity rebounded. The urban–rural LST differential broadened again to approximately 7.5 °C, with maximum urban LSTs exceeding 34 °C while rural surroundings remained comparatively cooler at 26 °C. This resurgence highlights the rapid return of anthropogenic drivers of SUHI as economic and social activities resumed (Figure 5c).

The results show that urban areas consistently exhibited higher LST than surrounding rural zones during all three periods. In 2019, the mean urban temperature exceeded the rural temperature by approximately 9 °C, representing the highest SUHI intensity observed in the study area. During the 2020 lockdown, both urban and rural LST values decreased, lowering the SUHI intensity to nearly 6 °C. This decline reflects reduced anthropogenic activity during the lockdown. In 2021, urban temperatures increased again, resulting in a SUHI intensity of approximately 8 °C, indicating a partial rebound of heat accumulation following the resumption of everyday activities.

Based on the temporal comparison, it was underscored that human activity strongly influences SUHI dynamics in Nowshera. The shrill cooling effect during the lockdown and subsequent rebound demonstrates the direct relationship between urban anthropogenic emissions and local thermal environments.

3.3. LST Variance Analysis Across Lockdown Phases

The impact of the COVID-19 lockdown on land surface temperature (LST) was assessed using a one-way ANOVA, with LST recorded on April 1 and April 20 across three distinct periods: Pre-Lockdown (2019), During Lockdown (2020), and post-lockdown (2021). The LST values for each date of the period and the average LST for each year were calculated to

yield an overall comparison table. The ANOVA test was performed to determine whether there were statistically significant differences in LST among the three periods. The null hypothesis (H$_0$) assumes no significant difference in mean LST across the periods, while the alternative hypothesis (H$_1$) suggests that at least one period exhibits a significant deviation. A significant level of 0.05 was used to evaluate the outcomes. The Table 3 below shows the LST obtained for 1st April and 20th April for three distinct periods.

Table 3. LST variation of pre, during, and post-lockdown periods in COVID-19 in Nowshera.

Period	Pre-Lockdown (2019)	During Lockdown (2020)	Post-Lockdown (2021)
April-01	31.45	25.4	31.55
April-20	31.31	25.28	31.47
Average	31.38 °C	25.34 °C	31.51 °C

The ANOVA test revealed a statistically significant difference in LST between the pre-lockdown, during-lockdown, and post-lockdown periods. The degree of freedom is F (2, 3) = 3691.46, and the *p*-value is <0.001. To further analyze which specific periods differed significantly, a Tukey HSD (Honestly Significant Difference) post hoc test was performed. The results of the Tukey HSD are presented in Table 4 below.

Table 4. Tukey HSD Test Results Comparing LST in Three Time Periods of Nowshera City.

Group 1	Group 2	Mean Difference	*p*-Adj	95% Confidence Interval	Reject H$_0$
During Lockdown	Post-Lockdown	6.17	<0.001	(5.8271, 6.5129)	True
During Lockdown	Pre-Lockdown	6.04	<0.001	(5.6971, 6.3829)	True
Post-Lockdown	Pre-Lockdown	−0.13	0.3763	(−0.4729, 0.2129)	False

Based on the Tukey HSD test, the following results were concluded:

1. The LST during the lockdown period was 6.17 °C lower than the post-lockdown period (*p* < 0.001).
2. The LST during the lockdown period was 6.04 °C lower than the pre-lockdown period (*p* < 0.001).
3. There was no significant difference in LST between the post-lockdown and pre-lockdown periods (*p* = 0.3763).

The assumption tests confirmed that the data met the criteria for one-way ANOVA. The Shapiro–Wilk test showed that LST values for all three periods followed a normal distribution (*p* > 0.05), and Levene's test indicated that the variances were homogeneous across groups (*p* > 0.05). After confirming these assumptions, the ANOVA results showed a statistically significant difference in mean LST across the pre-lockdown, lockdown, and post-lockdown years (*p* < 0.05). These findings validate the temporal differences in LST identified in the study.

The ANOVA and Tukey HSD tests indicated that the lockdown period had a significant impact on land surface temperature (LST). The LST during the lockdown was significantly lower than the pre-lockdown and post-lockdown periods. This advocates that reduced human activities, such as decreased industrial operations, transportation, and urbanization, contributed to a measurable cooling effect on the environment. The LST returned to near pre-lockdown levels after the lockdown, indicating that the cooling effect was temporary and dependent on the reduced activity levels during the lockdown.

3.4. Influence of LULC on LST

The land surface temperature (LST) over land use land cover (LULC) before, during, and after the COVID-19 lockdown has been determined and shown in Table 5 and Figure 6. The analysis reveals a diverse correlation between LULC and LST, underscoring the lockdown period's significance in shaping thermal patterns in Nowshera. On 15 April 2019, before the lockdown, the highest LST of 35.53 °C was observed in rangelands, while the lowest LST of 28.85 °C was recorded in water bodies. Similarly, during the 15 April 2020, lockdown, a noticeable decrease in LST across all LULC classes was observed. For example, the LST of rangelands dropped to 28.90 °C, and in water bodies, it reduced to 23.49 °C, showing the effect of the cessation of human activities on cooling. However, on 15 April 2021, after the lockdown, the LST rebounded, reaching 39.09 °C in rangelands and 31.10 °C in water bodies, signaling a revival in human activities and associated thermal emissions. Similarly, the built-up areas, characterized by densely populated settlements and infrastructure, had an average LST of 34.18 °C before the lockdown, which dropped to 26.8 °C during the lockdown but increased significantly to 35.36 °C afterwards. Similarly, rangelands showed a comparable trend, with an average LST of 35.53 °C before the lockdown, decreasing to 27.26 °C during the lockdown, and then climbing to 37.09 °C post-lockdown. Agricultural lands and vegetation cover followed a similar trajectory, with average LST values decreasing during the lockdown and then rising. Agricultural land, for instance, had an LST of 31.83 °C before the lockdown, which decreased to 24.54 °C during the lockdown and then rose to 32.52 °C afterwards. The LST of the vegetation cover was 33.32 °C before the lockdown, 24.27 °C during the lockdown, and 34.68 °C after the lockdown. Throughout all periods, water bodies continuously maintained the lowest LST, with pre-lockdown temperatures of 30.50 °C, lockdown temperatures of 24.20 °C, and post-lockdown temperatures of 32.69 °C. The spatial analysis of LST maps reveals distinct thermal hotspots concentrated within the densest built-up zones, particularly along major transportation corridors and commercial clusters. Cooler zones remain concentrated in agricultural and vegetated areas at the city's periphery. The comparison across the three years shows a clear contraction of cooler surfaces during the lockdown year, followed by the re-emergence of hotter zones in 2021. These spatial variations closely align with LULC patterns, particularly the dominance of impervious surfaces and the reduction in vegetation cover, as shown in Table 5 and Figure 6.

Table 5. District Nowshera, LST derived for various LULCC in April 2019, 2020, and 2021.

LULC Classes	Average Land Surface Temperature °C		
	April 2019	April 2020	April 2021
Built-Up Area	34.18	26.8	35.36
Rangeland	35.53	27.26	37.09
Agriculture land	31.83	24.54	32.52
Vegetation Cover	33.32	24.27	34.68
Water Bodies	30.5	24.2	32.69

This analysis shows that human activities have a significant impact on Nowshera's thermal environment, as demonstrated by the decrease in LST during the lockdown and the subsequent increase in the post-lockdown. The cooling effect was supported by the temporary halt in activities during the lockdown, which decreased anthropogenic heat emissions and vehicular activity.

Conversely, the rebound in LST post-lockdown indicates a resumption of human activities and the thermal emissions associated with them. The findings show that the provision of green spaces, optimal land use, and the regulation of emissions will influence

the region's climate and, hence, offer potential strategies to address urban heat challenges and enhance environmental resilience in rapidly urbanizing regions.

The NDVI, NDBI, and NDWI indices were analyzed to examine their relationship with spatial temperature patterns across the study area. A clear and consistent trend was observed in all three years. Areas with higher NDVI values (dense vegetation and irrigated agricultural zones) showed lower LST, reflecting the cooling influence of evapotranspiration. In contrast, zones with high NDBI values, representing built-up and impervious surfaces, consistently exhibited higher LST, confirming their role in intensifying surface heating. Water bodies, indicated by high NDWI values, showed the lowest temperatures among all land-cover types.

These relationships were further examined using zonal statistics, which showed negative correlations between NDVI and LST and positive correlations between NDBI and LST across all three periods. This pattern remained stable in the pre-lockdown, lockdown, and post-lockdown years and supports the interpretation that vegetation loss and built-up expansion significantly influence surface heating in the district.
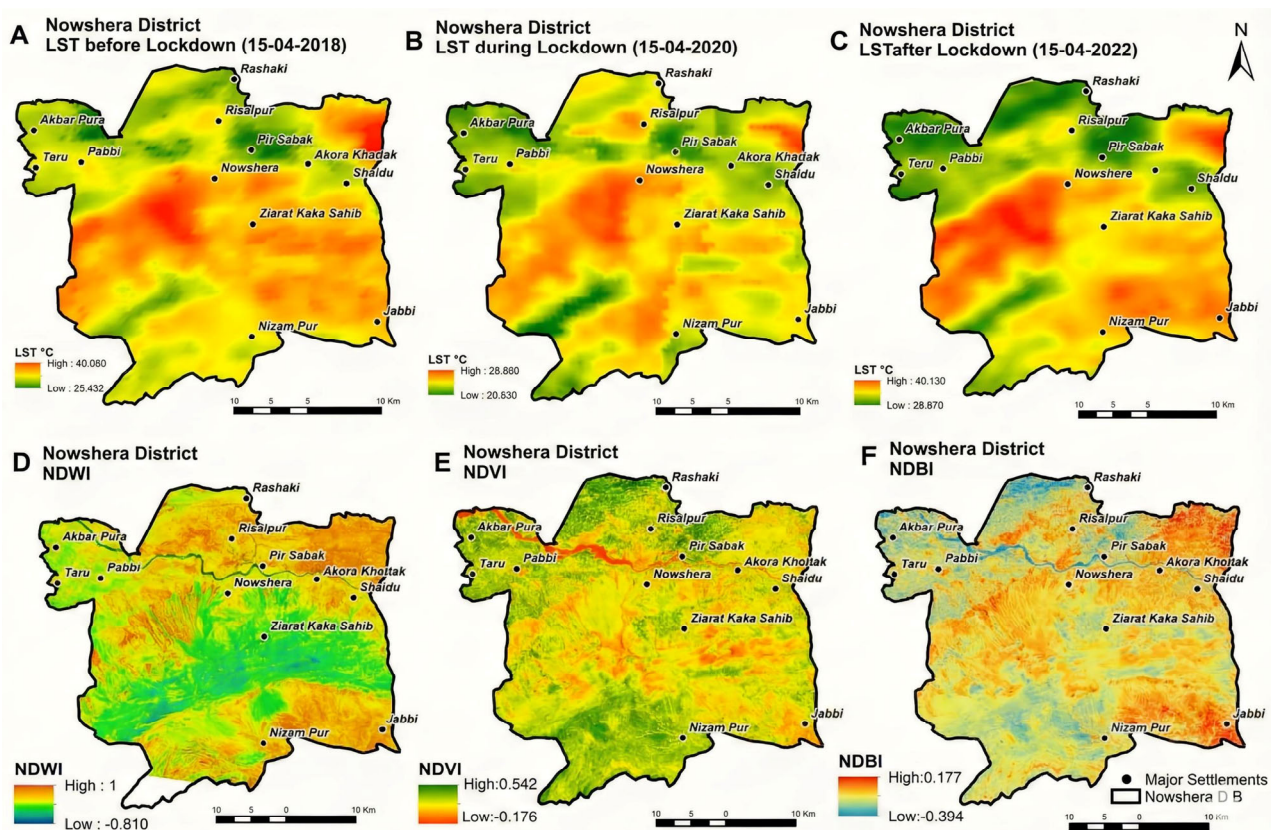

Figure 6. (**A**) LST derived on 04-2019, (**B**) LST derived on 04-2020, (**C**) LST derived on 04-2021, (**D**) Normalized Difference Water Index (NDWI), (**E**) Normalized Difference Vegetation Index (NDVI), and (**F**) Normalized Difference Built-Up Index (NDBI) of the study area.

Figure 5 illustrates LULC and LST in the pre-, during, and post-pandemic periods. Figure 6 shows the different indices in the pre-, during, and post-pandemic periods. Figure 7 shows the Land Use/Land Cover (LULC) distribution and corresponding land surface temperature (LST) patterns for the study area.
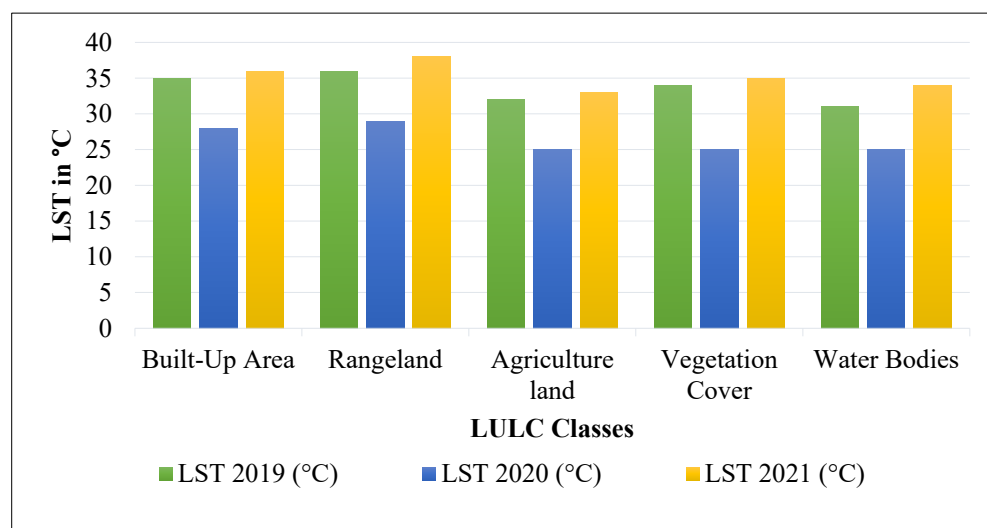
Figure 7. Land Use/Land Cover (LULC) distribution and corresponding land surface temperature (LST) patterns for the study area.

4. Discussion

This study comprehensively examined the surface urban heat island (SUHI) effect and land surface temperature (LST) variations in the Nowshera district before, during, and after the COVID-19-induced lockdown. The findings provide critical insights into how anthropogenic activities impact urban thermal environments and how temporary disruptions in human activity can mitigate the effects of urban heat.

4.1. SUHI Dynamics Across Lockdown Phases

The dynamics of the SUHI in Nowshera city exhibit distinct temporal variations across the pre-lockdown, and post-lockdown periods, closely reflecting variations in human activity.

During the pre-lockdown phase (April 2019), the SUHI effect was strongly developed, with an urban–rural thermal difference of nearly 9 °C. The urban core reached about 36 °C, while suburban and rural areas recorded about 27 °C. This pronounced gradient highlights the role of dense built-up structures, traffic congestion, and limited vegetation in driving intense heat accumulation.

In the lockdown period (April 2020), SUHI intensity declined noticeably to around 6 °C. Urban areas averaged 30 °C, compared with 24 °C in rural regions. This reduction corresponds to the cooling effects of reduced anthropogenic activities, including lower vehicular traffic, delayed industrial operations, and reduced energy use. Similar reductions were documented in other global cities during COVID-19 restrictions, where decreases in human activity not only lowered urban heat intensity but also improved air quality by reducing NO_2, SO_2, and particulate matter.

By the post-lockdown phase (April 2021), the SUHI effect rebounded, with the urban–rural differential widening again to approximately 7.5 °C. Maximum LSTs in the urban core exceeded 34 °C, while rural surroundings remained relatively cooler at 26 °C. This resurgence reflects the rapid return of anthropogenic heat sources as economic and social activities resumed, reinstating pre-pandemic thermal stress conditions.

As a whole, the three stages underscore SUHI's sensitivity to human-driven processes. The lockdown acted as a unique natural experiment, demonstrating that temporary reductions in anthropogenic activity can significantly mitigate urban heat. However, the swift rebound of SUHI post-lockdown underscores the unsustainability of these effects and underscores the need for structural, long-term strategies to curb urban heat. Interventions such as increasing urban vegetation, adopting reflective and permeable surfaces, and re-

ducing vehicular and industrial emissions represent more sustainable solutions to address the intensification of urban thermal environments.

Driving Factors of SUHI

The intensity of the surface urban heat island (SUHI) effect in Nowshera varies significantly over time and space, driven by a complex interplay of human activities and natural factors. This dynamic relationship underscores the critical importance of understanding both anthropogenic influences and biophysical conditions to effectively address and mitigate urban heat impacts in the region. During the COVID-19 lockdown (2020), a marked reduction in traffic flows, industrial activity, and associated anthropogenic heat emissions likely contributed to the observed decline in SUHI intensity. Similar reductions in urban heat linked to decreased economic activity during lockdown periods have been reported in other regions [35,36].

Vegetation also played a significant role in SUHI dynamics. The observed increase in NDVI values during the lockdown period indicates that vegetation health and coverage improved, possibly due to reduced air pollution and human disturbances. This expansion of green cover increased evapotranspiration, which, in turn, mitigated surface heating. Previous studies confirm that vegetation density is a key cooling driver in regulating SUHI effects [37,38].

Conversely, the pre-lockdown (2019) and post-lockdown (2021) phases highlighted the role of population density and built-up expansion in driving higher baseline SUHI intensities. As impervious surfaces expand and compact urban forms dominate, the city's thermal capacity increases, leading to more pronounced heat-island effects. This aligns with global findings that rapid urbanization and land-use change are principal drivers of SUHI development, particularly in medium-sized cities of developing countries [39,40].

Thus, SUHI in Nowshera appears to be shaped by a combination of reduced anthropogenic heat during lockdown, vegetation recovery, and long-term pressure from urban growth. These highlight the importance of balanced land-use planning, strict air-quality regulations, and green infrastructure development in mitigating future urban heat.

Similarly, the ANOVA and Tukey HSD tests reveal significant differences in land surface temperature (LST) across the pre-lockdown, lockdown, and post-lockdown periods. The ANOVA test ($F_{(2, 3)}$ =3691.46, $p = 0.001$) indicates that at least two of the period's LST values are significantly different. The Tukey HSD post hoc test further indicates that during the lockdown period, LST was significantly lower than in the pre-lockdown ($p < 0.001$) and post-lockdown ($p < 0.001$) periods. This demonstrates that reduced human activities during the lockdown, such as decreased industrial and transportation operations, contributed to the cooling effect of the environment. However, the lack of significant difference between the pre-lockdown and post-lockdown periods ($p = 0.3763$) indicates that the cooling effect was temporary, with LST returning to near-normal levels after restrictions were lifted. These findings highlight the potential benefits of reducing human activities on the overall city environment.

Although ANOVA and Tukey HSD provide a robust statistical basis for testing differences in LST across the three study periods, more advanced spatial or multivariate models, such as Multiple Linear Regression (MLR) or Geographically Weighted Regression (GWR), could further explain the spatial determinants of LST variation. Incorporating such techniques would enable a deeper analysis of how land covers, built-up density, vegetation patterns, or elevation contribute to LST distribution. These approaches are recommended for future studies aiming to model LST drivers rather than to compare temporal changes.

4.2. LST and LULC Relationships

A detailed investigation of the relationship between LST and various Land Use/Land Cover (LULC) classes further reinforces the critical role of land cover in moderating urban temperatures. The findings indicate that built-up areas and rangelands consistently recorded the highest LST values, while vegetated and water bodies maintained relatively lower temperatures. During the lockdown, the cooling effect was particularly pronounced in built-up areas and rangelands, where the cessation of anthropogenic heat sources led to notable temperature declines. The reduction of industrial emissions and diminished vehicular traffic likely played a pivotal role in this cooling trend. Conversely, water bodies exhibited minimal change, maintaining their role as natural cooling elements in the urban landscape. The post-lockdown period witnessed a rapid rebound in LST values across built-up and rangeland areas, suggesting that human activities resumed at higher intensity. This pattern demonstrates the challenge of maintaining thermal stability in urban areas under traditional development paradigms that prioritize impervious surfaces and limited vegetation.

The findings demonstrate that the COVID-19 lockdown significantly reduced land surface temperature (LST) and the intensity of the surface urban heat island (SUHI) in Nowshera, a secondary city in Pakistan. While similar cooling effects have been documented in global metropolitan contexts such as Wuhan, China [41], Delhi, India [42], and Milan, Italy [43]. This study is unique in extending the analysis to a mid-sized South Asian urban setting that is rarely represented in SUHI literature.

While the spatial maps reveal visible patterns of thermal clustering, future studies may apply spatial statistics, such as the Getis–Ord Gi* hotspot analysis, to identify statistically significant high- and low-temperature clusters. Such techniques would enable a more formal assessment of hotspot persistence and spatial autocorrelation, complementing the temporal and LULC-based interpretation presented in this study.

The novelty of this research lies in revealing that the relationship between reduced anthropogenic activity and urban heat mitigation is not limited to megacities. In Nowshera, decreased traffic flow, industrial slowdown, and reduced commercial operations during lockdown resulted in a noticeable decline in LST and SUHI. This demonstrates that even secondary cities—where rapid urban growth often weakens governance capacity—exhibit measurable climate responses to shifts in human mobility and energy use.

Furthermore, this study provides localized evidence for Pakistan, a country where most SUHI research has concentrated on megacities such as Lahore [44] and Karachi [45]. By focusing on Nowshera, this study highlights that mid-sized cities, projected to absorb most of the urban population growth in South Asia [46], are equally vulnerable to urban heat risks but also hold untapped opportunities for sustainable urban planning.

The implications of this study extend beyond Nowshera. The observed cooling during lockdown suggests that targeted interventions, such as traffic demand management, green infrastructure, and compact energy-efficient urban design, could deliver similar benefits without requiring extreme mobility restrictions. This strengthens the argument for integrating climate-sensitive policies into urban planning in secondary cities of Pakistan and other developing countries, where climate adaptation strategies often prioritize only larger metropolitan regions.

This study provides several contributions that extend beyond the existing SUHI literature. First, unlike most SUHI studies that focus on long-term urbanization trends, this research examines how an abrupt and unprecedented reduction in human activity during the COVID-19 lockdown influenced surface temperatures. This offers a unique opportunity to isolate the impact of anthropogenic activity from broader climatic or seasonal variations. Second, the study integrates LULC classification, SUHI intensity mapping, and seasonal

LST comparisons to examine how short-term changes in mobility and emissions correspond to thermal behavior across different land cover types. Such an approach is less common in previous SUHI studies, which often rely on single-period analyses. Third, the study area, medium-sized cities in a developing region, represents an understudied urban context in global SUHI literature. Much of the existing research focuses on large metropolitan cities, leaving gaps in understanding how SUHI responds to human-activity shocks in smaller, rapidly urbanizing environments. By addressing this gap, the study offers new insights into SUHI dynamics in regions with limited data availability and environmental monitoring.

5. Limitations and Future Directions

This study provides valuable insights into the impacts of the COVID-19 lockdown on land surface temperature (LST) and surface urban heat island (SUHI) intensity in Nowshera, Pakistan. However, several limitations must be acknowledged. First, the analysis is based on Landsat-derived LST, which provides daytime measurements and captures the nocturnal surface urban heat island (SUHI) effect, which is typically most pronounced then. Future studies should incorporate nighttime thermal data from Landsat's Thermal Infrared Sensor (TIRS), which can capture nighttime thermal signals. Suitable nighttime scenes for the study years were not available with acceptable cloud-free conditions. For this reason, the analysis in this study is based only on daytime LST. While daytime observations are sufficient for detecting SUHI patterns, incorporating nighttime thermal data in future research would allow a more complete understanding of diurnal heat island dynamics. Second, the spatial and temporal resolution of Landsat, while adequate for localized analysis, may not fully capture short-term or fine-scale variations in thermal conditions. Higher-resolution imagery, such as from Sentinel-3 SLSTR or commercial satellites, could improve the robustness of findings.

The study relies on a single cloud-free Landsat image per period due to limited data availability during the selected months. While these scenes were chosen to ensure consistent seasonal conditions, future studies could integrate multi-date or seasonal LST composites to further reduce weather-related bias.

Methodologically, the study employed a conventional SUHI estimation approach based primarily on temperature differences. While this provides a valuable baseline, more sophisticated statistical or machine-learning approaches could be employed to disentangle the complex interplay among land use, vegetation cover, and anthropogenic activities in driving SUHI intensity. Additionally, due to data limitations, the study did not incorporate atmospheric pollutants (e.g., NO_2, SO_2, CO, and Aerosol Optical Depth) that significantly influence surface heating and cooling dynamics, particularly during the lockdown when emissions patterns were altered. Future research should integrate air quality indicators and socio-economic activity datasets (e.g., traffic flow, industrial activity indices, or energy consumption) to strengthen causal inferences.

Although remote sensing data and statistical analysis were used to study land surface temperature and vegetation dynamics, no ground-truth data, such as in-situ LST measurements from local weather stations or field surveys, were collected. The absence of ground validation may limit the precision of the satellite-derived estimates. Future research should integrate field-based observations with remote sensing datasets to enhance the accuracy and robustness of urban climate assessments.

Similarly, the focus on temporal variation in LST under lockdown conditions led to the use of ANOVA and Tukey's HSD to test differences among the three periods. Future research may extend this work by applying multivariate or spatially explicit models (e.g., MLR or GWR) to explore the spatial drivers of LST further.

The spatial interpretation of LST patterns using classified maps and SUHI gradients. Incorporating statistical hotspot analysis (e.g., Getis–Ord Gi*) could enhance future research by quantifying the significance of thermal clusters.

This study also acknowledges uncertainties in LST retrieval, atmospheric correction, and LULC classification. These were minimized using standardized correction workflows and validated classification procedures; however, future research may incorporate dedicated uncertainty modeling for more detailed quantification.

Lastly, this study focused on a medium-sized city in Pakistan, which limits the generalizability of the results. Comparative multi-city analyses across varying urban morphologies and climatic contexts would enhance the broader applicability of findings. Future studies should also extend the temporal scope beyond the lockdown period to assess post-pandemic recovery patterns in LST and SUHI trends, providing more holistic evidence on the long-term implications of reduced anthropogenic activity for urban thermal environments.

6. Conclusions

This study explored the variations in land surface temperature (LST) and the surface urban heat island (SUHI) effect in the Nowshera district before, during, and after the COVID-19 lockdown, providing the first empirical evidence from a secondary city in Khyber Pakhtunkhwa, Pakistan. The analysis revealed that reductions in anthropogenic activities, particularly traffic and industrial operations, led to measurable changes in the thermal environment. Specifically, during the lockdown period, urban LST dropped significantly, highlighting the direct link between human activities and urban heat dynamics. This cooling effect was most evident near major transportation corridors and metropolitan zones where reductions in vehicular flow were most pronounced. The results further demonstrated that before the lockdown (2019), Nowshera experienced a strongly pronounced SUHI effect, with urban–rural temperature differences reaching nearly 9 °C. The lockdown, however, resulted in a sharp reduction in this gradient to about 6 °C, underscoring how curtailed human mobility and industrial activity reduced anthropogenic heat emissions. After restrictions were lifted (2021), LSTs and SUHI intensity rebounded, reaching nearly 7.5 °C of differential, reflecting the rapid recovery of urban heat once economic and social activities resumed. This clear temporal trajectory emphasizes the dynamic role of human behavior in shaping local heating environments.

By examining the relationship between LST and Land Use/Land Cover (LULC), the study also confirmed that built-up areas contributed most to SUHI intensity due to their heat-absorbing properties. At the same time, green spaces and water bodies consistently acted as cooling zones. This highlights vegetation's ecological role in moderating heat stress and provides practical evidence for integrating green infrastructure into urban planning. In addition, the study demonstrates methodological innovation by using multi-temporal Landsat-derived LST to capture SUHI variations at a local scale in a mid-sized South Asian city, a context rarely addressed in the existing literature.

In short, the study makes several key contributions: (i) it is among the first to link COVID-19 lockdown-related mobility restrictions with SUHI dynamics in a secondary Pakistani city, moving beyond the focus on megacities; (ii) it empirically demonstrates the scale of cooling associated with reduced anthropogenic heat emissions, thereby strengthening the evidence base for sustainable urban heat mitigation; and (iii) it advances policy implications by showing that while temporary reductions in human activity can significantly reduce SUHI, long-term resilience requires structural interventions such as expanding urban green cover, adopting reflective building materials, and promoting energy-efficient urban design. The findings not only document a unique natural experiment in Nowshera but also

contribute regionally and internationally to the growing understanding of human–urban climate interactions.

References

1. Fu, P.; Weng, Q. A Time Series Analysis of Urbanization Induced Land Use and Land Cover Change and Its Impact on Land Surface Temperature with Landsat Imagery. *Remote Sens. Environ.* **2016**, *175*, 205–214. [CrossRef]
2. Zhang, S.; Zhu, H.; Zeng, K.; Zhang, Y.; Jin, Z.; Wang, Y.; Zhang, R.; Jürgen, B.; Liu, M. From City to Countryside: Unraveling the Long-Term Complex Effects of Urbanization on Vegetation Growth in China. *J. Environ. Manag.* **2025**, *380*, 124975. [CrossRef]
3. Ibrahim, M.; Nasir, M.J. Unraveling the Complexities of Land-Use–Land Cover Transformation and Its Impact on Land Surface Temperature and Urban Heat Island Effect: A Study of Nowshera District, Pakistan. *J. Urban Plan. Dev.* **2024**, *150*, 4024031. [CrossRef]
4. Ibrahim, M.; Ahmad, N. Quantitative Evaluation and Challenges Confronting Dedicated Green Spaces in Cities: A Case Study of Peshawar, Pakistan. *Geol. Ecol. Landsc.* **2023**, *9*, 706–717. [CrossRef]
5. Zhong, S.; Qian, Y.; Zhao, C.; Leung, R.; Wang, H.; Yang, B.; Fan, J.; Yan, H.; Yang, X.-Q.; Liu, D. Urbanization-Induced Urban Heat Island and Aerosol Effects on Climate Extremes in the Yangtze River Delta Region of China. *Atmos. Chem. Phys.* **2017**, *17*, 5439–5457. [CrossRef]
6. Ho, J.Y.; Shi, Y.; Lau, K.K.L.; Ng, E.Y.Y.; Ren, C.; Goggins, W.B. Urban Heat Island Effect-Related Mortality under Extreme Heat and Non-Extreme Heat Scenarios: A 2010–2019 Case Study in Hong Kong. *Sci. Total Environ.* **2023**, *858*, 159791. [CrossRef]
7. Shahjahan, A.T.M. Urban Adaptation Measures for Climate Change: Study of Urban Wetlands in View of Potential Urban Cooling. Master's Thesis, Bangladesh University of Engineering and Technology (BUET), Dhaka, Bangladesh, 2018.
8. Sodiq, A.; Baloch, A.A.B.; Khan, S.A.; Sezer, N.; Mahmoud, S.; Jama, M.; Abdelaal, A. Towards Modern Sustainable Cities: Review of Sustainability Principles and Trends. *J. Clean. Prod.* **2019**, *227*, 972–1001. [CrossRef]
9. Naeem, W.; Kim, J.; Lee, Y.G. Spatiotemporal Variations in the Air Pollutant NO_2 in Some Regions of Pakistan, India, China, and Korea, before and after COVID-19, Based on Ozone Monitoring Instrument Data. *Atmosphere* **2022**, *13*, 986. [CrossRef]
10. Kim, K. Impacts of COVID-19 on Transportation: Summary and Synthesis of Interdisciplinary Research. *Transp. Res. Interdiscip. Perspect.* **2021**, *9*, 100305. [CrossRef]
11. Kandukuri, K. Impact of Environmental Variables on COVID-19—A Study from the Telangana State, India. *Biom. Biostat. Int. J.* **2024**, *13*, 36–40. [CrossRef]
12. Shamshudin, F.; Daud, N.R. Monitoring Effects of Lockdown during COVID-19 Pandemic towards the Air Pollution in Southeast Asia/Nurul Fathimah Shamshudin and Nurul Rabitah Daud. *J. Sustain. Civ. Eng. Technol.* **2022**, *1*, 29–42. [CrossRef]
13. Zajfert, M. Urban Transport during the COVID-19 Pandemic: A Case Study of Poland. *Public Transp.* **2025**, *17*, 153–176. [CrossRef]
14. Bechtel, B.; Demuzere, M.; Mills, G.; Zhan, W.; Sismanidis, P.; Small, C.; Voogt, J. SUHI Analysis Using Local Climate Zones—A Comparison of 50 Cities. *Urban Clim.* **2019**, *28*, 100451. [CrossRef]
15. Kara, Y.; Yavuz, V.; Lupo, A.R. Multi-Index Assessment of Surface Urban Heat Island (SUHI) Dynamics in Samsun Using Google Earth Engine. *Atmosphere* **2025**, *16*, 712. [CrossRef]

16. Firozjaei, M.K.; Fathololomi, S.; Kiavarz, M.; Arsanjani, J.J.; Homaee, M.; Alavipanah, S.K. Modeling the Impact of the COVID-19 Lockdowns on Urban Surface Ecological Status: A Case Study of Milan and Wuhan Cities. *J. Environ. Manag.* **2021**, *286*, 112236. [CrossRef]

17. Azmeer, A.; Tahir, F.; Al-Ghamdi, S.G. Progress on Green Infrastructure for Urban Cooling: Evaluating Techniques, Design Strategies, and Benefits. *Urban Clim.* **2024**, *56*, 102077. [CrossRef]

18. Huang, X.; Wang, Y. Investigating the Effects of 3D Urban Morphology on the Surface Urban Heat Island Effect in Urban Functional Zones by Using High-Resolution Remote Sensing Data: A Case Study of Wuhan, Central China. *ISPRS J. Photogramm. Remote Sens.* **2019**, *152*, 119–131. [CrossRef]

19. Trlica, A.; Hutyra, L.R.; Schaaf, C.L.; Erb, A.; Wang, J.A. Albedo, Land Cover, and Daytime Surface Temperature Variation across an Urbanized Landscape. *Earth's Future* **2017**, *5*, 1084–1101. [CrossRef]

20. Smith, I.A.; Fabian, M.P.; Hutyra, L.R. Urban Green Space and Albedo Impacts on Surface Temperature across Seven United States Cities. *Sci. Total Environ.* **2023**, *857*, 159663. [CrossRef]

21. Rotem-Mindali, O.; Michael, Y.; Helman, D.; Lensky, I.M. The Role of Local Land-Use on the Urban Heat Island Effect of Tel Aviv as Assessed from Satellite Remote Sensing. *Appl. Geogr.* **2015**, *56*, 145–153. [CrossRef]

22. Ibrahim, M.; Ahmad, N.; Mahar, W.A.; Nasir, M.J. Assessment of the Spatial Inequality and Configuration of Recreational Green Spaces in the Urban Centre of Nowshera, Pakistan. *Discov. Cities* **2025**, *2*, 113. [CrossRef]

23. USGS USGS: Landsat Collection 2 Level-1 Data Products. Available online: https://earthexplorer.usgs.gov (accessed on 22 November 2025).

24. Gao, M.; Qin, Z.; Qiu, J.; Liu, S.; Xu, B.; Li, W.; Yang, X. Retrieving Spatial-Temporal Variation of Land Surface Temperature in Tibetan Plateau for the Years 2005-2006 from MODIS Satellite Data. In Proceedings of the SPIE Remote Sensing, Cardiff, UK, 14–18 September 2008; Volume 7110, pp. 348–357.

25. Li, Z.L.; Wu, H.; Wang, N.; Qiu, S.; Sobrino, J.A.; Wan, Z.; Tang, B.H.; Yan, G. Land surface emissivity retrieval from satellite data. *Int. J. Remote Sens.* **2013**, *34*, 3084–3127. [CrossRef]

26. Ashwini, K.; Sil, B.S.; Kafy, A.A.; Altuwaijri, H.A.; Nath, H.; Rahaman, Z.A. Harnessing Machine Learning Algorithms to Model the Association between Land Use/Land Cover Change and Heatwave Dynamics for Enhanced Environmental Management. *Land* **2024**, *13*, 1273. [CrossRef]

27. Gandhi, G.M.; Parthiban, S.; Thummalu, N.; Christy, A. Ndvi: Vegetation Change Detection Using Remote Sensing and Gis—A Case Study of Vellore District. *Procedia Comput. Sci.* **2015**, *57*, 1199–1210. [CrossRef]

28. Johansen, B.; Tømmervik, H. The Relationship between Phytomass, NDVI and Vegetation Communities on Svalbard. *Int. J. Appl. Earth Obs. Geoinf.* **2014**, *27*, 20–30. [CrossRef]

29. Guha, S.; Govil, H.; Diwan, P. Analytical Study of Seasonal Variability in Land Surface Temperature with Normalized Difference Vegetation Index, Normalized Difference Water Index, Normalized Difference Built-up Index, and Normalized Multiband Drought Index. *J. Appl. Remote Sens.* **2019**, *13*, 24518.

30. Chen, X.; Cao, X.; Liao, A.; Chen, L.; Peng, S.; Lu, M.; Chen, J.; Zhang, W.; Zhang, H.; Han, G. Global Mapping of Artificial Surfaces at 30-m Resolution. *Sci. China Earth Sci.* **2016**, *59*, 2295–2306. [CrossRef]

31. Zhao, H.R.; Shi, H.; Yang, H.; Li, X.W.; Wang, J.D.; Zhang, X. Separating the Radiance Contribution of Land Surface and Atmosphere. In Proceedings of the IGARSS 2003. 2003 IEEE International Geoscience and Remote Sensing Symposium, Toulouse, France, 21–25 July 2003; Proceedings (IEEE Cat. No. 03CH37477). IEEE: Piscataway, NJ, USA, 2003; Volume 6, pp. 3878–3880.

32. Sresto, M.A.; Siddika, S.; Fattah, M.A.; Morshed, S.R.; Morshed, M.M. A GIS and Remote Sensing Approach for Measuring Summer-Winter Variation of Land Use and Land Cover Indices and Surface Temperature in Dhaka District, Bangladesh. *Heliyon* **2022**, *8*, e10309. [CrossRef]

33. Zhao, H.; Chen, X. Use of Normalized Difference Bareness Index in Quickly Mapping Bare Areas from TM/ETM+. In Proceedings of the International Geoscience and Remote Sensing Symposium, Seoul, Republic of Korea, 24–29 July 2005; Volume 3, p. 1666.

34. Imran, H.M.; Hossain, A.; Islam, A.K.M.S.; Rahman, A.; Bhuiyan, M.A.E.; Paul, S.; Alam, A. Impact of Land Cover Changes on Land Surface Temperature and Human Thermal Comfort in Dhaka City of Bangladesh. *Earth Syst. Environ.* **2021**, *5*, 667–693. [CrossRef]

35. Chakraborty, T.C.; Sarangi, C.; Lee, X. Reduction in Human Activity Can Enhance the Urban Heat Island: Insights from the COVID-19 Lockdown. *Environ. Res. Lett.* **2021**, *16*, 54060. [CrossRef]

36. Feng, Z.; Wang, X.; Yuan, J.; Zhang, Y.; Yu, M. Changes in Air Pollution, Land Surface Temperature, and Urban Heat Islands during the COVID-19 Lockdown in Three Chinese Urban Agglomerations. *Sci. Total Environ.* **2023**, *892*, 164496. [CrossRef]

37. Li, L.; Zha, Y.; Zhang, J. Spatially Non-Stationary Effect of Underlying Driving Factors on Surface Urban Heat Islands in Global Major Cities. *Int. J. Appl. Earth Obs. Geoinf.* **2020**, *90*, 102131. [CrossRef]

38. Li, L.; Zha, Y. Satellite-Based Spatiotemporal Trends of Canopy Urban Heat Islands and Associated Drivers in China's 32 Major Cities. *Remote Sens.* **2019**, *11*, 102. [CrossRef]

39. Doulay Seydou, K.; Morenikeji, W.; Diouf, A.; Dicko, K.; Erdanaev, E.; Loewner, R.; Okhimamhe, A.A. Dynamics of Zinder's Urban Landscape: Implications for Sustainable Land Use Management and Environmental Conservation. *Sustainability* **2024**, *16*, 10263. [CrossRef]

40. Moazzam, M.F.U.; Lee, B.G. Urbanization Influenced SUHI Of 41 Megacities of the World Using Big Geospatial Data Assisted with Google Earth Engine. *Sustain. Cities Soc.* **2024**, *101*, 105095. [CrossRef]

41. Wang, R.; Wang, M.; Zhang, Z.; Hu, T.; Xing, J.; He, Z.; Liu, X. Geographical Detection of Urban Thermal Environment Based on the Local Climate Zones: A Case Study in Wuhan, China. *Remote Sens.* **2022**, *14*, 1067. [CrossRef]

42. Dutta, D.; Rahman, A.; Paul, S.K.; Kundu, A. Changing Pattern of Urban Landscape and Its Effect on Land Surface Temperature in and around Delhi. *Environ. Monit. Assess.* **2019**, *191*, 551. [CrossRef]

43. Puche, M.; Vavassori, A.; Brovelli, M.A. Insights into the Effect of Urban Morphology and Land Cover on Land Surface and Air Temperatures in the Metropolitan City of Milan (Italy) Using Satellite Imagery and in Situ Measurements. *Remote Sens.* **2023**, *15*, 733. [CrossRef]

44. Arsalan, M. Surface Urban Heat Island (SUHI) Pattern and Trends in Main Cities of Pakistan: Lahore and Faisalabad. *Environ. Sci. Ecol. Curr. Res.* **2025**, *6*, 10112. [CrossRef]

45. Rizvi, S.H.; Fatima, H.; Iqbal, M.J.; Alam, K. The Effect of Urbanization on the Intensification of SUHIs: Analysis by LULC on Karachi. *J. Atmos. Sol. Terr. Phys.* **2020**, *207*, 105374. [CrossRef]

46. UN-Habitat. *World Cities Report 2022: Envisaging the Future of Cities*; UN-Habitat: Nairobi, Kenya, 2022.